RESEARCH ARTICLE

WILEY

Adaptive neural tracking control for flexible joint robot including hydraulic actuator dynamics with disturbance observer

Van Du Phan[1] | Cong Phat Vo[2] | Kyoung Kwan Ahn[3]

[1]School of Engineering and Technology, Vinh University, Vinh, Vietnam

[2]Autonomous Robot 24Hours 7Days Co., Ltd, Gyeonggi-do, South Korea

[3]School of Mechanical Engineering, University of Ulsan, Ulsan, South Korea

Correspondence
Kyoung Kwan Ahn, School of Mechanical Engineering, University of Ulsan, Ulsan 44610, South Korea.
Email: kkahn@ulsan.ac.kr

Abstract

In this paper, a disturbance observer-based adaptive neural backstepping integral sliding mode control (BISMC) is developed for a flexible joint robot (FJR) with the integration of an adjustable stiffness rotary actuator (ASRA). This system suffers from unknown system dynamics, external disturbance, and the influence of variable stiffness, which is a challenge for achieving precision tracking performance. Considering the lumped disturbances in FJR generated by the hydraulic system and the stiffness modulation of the ASRA, we investigate the structural dynamics nonlinear model of the FJR system, including hydraulic actuator dynamics. While other linear control strategies are applied for the FJR, the proposed controller uses BISMC, neural networks (NN), and nonlinear disturbance observers to deal with the disadvantages mentioned above. Radial basis function neural networks (RBFNN) are designed to tackle unknown nonlinear functions, and the disturbance observers are introduced to compensate for the influence of the variable stiffness, disturbance, and the approximation error caused by NN. Simulations and experiments are independently implemented to demonstrate the effectiveness and feasibility of the proposed controller. Results exhibit that the integral absolute error-index is reduced by 20.4% when the proposed method is deployed for the experiment with a multistep trajectory.

KEYWORDS

adaptive control, disturbance observer, flexible joint robot, neural network, sliding mode, variable stiffness

1 | INTRODUCTION

In the evolution of robot, the soft robotic brings many promising breakthroughs such as collision safety, high accuracy, energy optimization, and flexibility.[1–4] The appearance of a compliance actuator helps to deal with the drawback of the conventional rigid joint. To be more specific, the stiffness features of the VSA (variable stiffness actuator) approach can

be regulated flexibly such that the FJR can adapt to the particular tasks. The injury level will be mitigated during robot manipulators interacting with humans in case of low stiffness. Meanwhile, the case of high stiffness is utilized to guarantee precision tracking control with low-velocity tasks. Several illustrations for VSA-based manipulator 1-degrees of freedom (DOF) are introduced like Compact-VSA, ASRA, serial VSA (SVSA), and so on in References 5–7. whereby the VSA uses two different motors to separately manipulate the stiffness and position. Besides, the hydraulic actuator also is designed for VSA due to its high power-to-weight ratio and a large force/torque generation.[8,9] However, in the literature survey on tracking control for VSA, actuator dynamics has been neglected to facilitate the design control process, leading to performance degradation as well as the system stability. An additional difficulty emerges due to the fact that hydraulic actuator suffers from heavy modeling uncertainties and highly nonlinear features, for instance, friction, complicated leakage properties, parameters variation and so on.[10,11] This is the reason why the actuator dynamics should be taken into account by the control design procedure. Many published studies developed different control strategies for practical tracking control of robotic systems with variable stiffness joints, that is, backstepping controller,[12] gain scheduling control,[13] feedback linearization (FBL) control,[14] prescribed performance control (PPC),[15] etc. Nonetheless, these approaches rely on linear modes of plants and do not cover the actuator dynamics as well as unknown nonlinear dynamic uncertainties. Thus, the output tracking problem of VSA, including hydraulic actuator dynamics brings more challenges, especially, in the simultaneous occurrence of the nonlinear uncertainty, matched, and mismatched disturbance.[16]

In order to cope with nonlinear features and unknown system dynamics, several approaches have been investigated in recent decades in which a neural network (NN) is an effective approach to approximate the unknown nonlinear function because of the self-learning capability.[17–24] The NNs require little relative information about the dynamics of the system. In References 17,18, an adaptive neural network controller is developed to resolve problems of unknown dynamics for robotic systems with variable stiffness joints. Besides, a NN controller is also constructed to ameliorate the robustness and suppress the vibration of a flexible robotic manipulator system in spite of input dead-zone and the unknown dynamics.[20] The other notable studies are investigated to handle the unknown dynamic system, such as a neural network-based feedback linearization technique for SVSA,[21] a neural network-based adaptive sliding mode control for a VSA,[22] etc. However, the big approximation error may appear when the approximated function does not depend on the system states or control input. Another reason causes the above-mentioned issue which is an unsuitable selection of the RBFNN architecture. These errors significantly attenuate the dynamic behavior and even instability phenomenon.

Since the approximation error of the NN, the external load, and the influence of the variable stiffness are hypothetical as the lumped disturbance, the development of the effectively advanced methods to deal with them has been discussed such as an adaptive robust controller and an observer-based composite controller. In References 9,25, the electrohydraulic elastic manipulator in the face of the matched and unmatched disturbances is presented whilst the negative influence of the disturbances is suppressed by the adaptive switching gain in the control law. In Reference 26, an adaptive robust controller based on fuzzy global coupled non-singular fast terminal sliding mode control was proposed for the n-rigid-link elastic-joint robot manipulators to reduce the impact of the lumped disturbances. However, in practical applications, the selection of a large gain coefficient may affect the system stability, as well as excites unmodeled dynamics and/or saturate the driver, leading to unsatisfactory performance. Meanwhile, the observer-based method has already been performed to eliminate the disturbance/uncertainty for the compliant actuators. In detail, the control performance of the system will be significantly enhanced as the estimated disturbance is compensated by the control design procedure. Several observers are introduced for the variable stiffness actuator by previous researches, such as nonlinear disturbance observer (NDO),[27,28] extend state observer,[29,30] impedance observer,[31] adaptive observer,[32] etc. However, the potential benefit of the NNs in combination with the observer-based nonlinear controller has still been an open problem. This perfect incorporation can simultaneously approximate the unknown dynamic system and eliminate the impact of the variable stiffness and disturbances. So, taking advantage of a hybrid controller with attached techniques like NN, NDO provides a promising way to promote the system performance for the variable stiffness actuator system.

Motivated by the above analysis, a new approach is developed for FJR with the integration of the ASRA, which includes the actuator dynamics in this work. One advantage of the suggested method is that, by combining the nonlinear disturbance observers, and the RBFNN approximator with backstepping integral sliding mode technique, the proposed control can deal with the unknown nonlinear dynamic system, the impacts of variable stiffness, as well as external disturbance. In addition, the suggested controller not only assures the stability of the controlled system but also

tracks the desired trajectory with a good performance. In summary, the main contribution of this paper can be shown as follow:

1. The FJR mathematical model, encompassing hydraulic actuator dynamics, is initially formulated, where factors affecting both mechanical and hydraulic dynamics are consolidated into matched and mismatched disturbances.
2. To the best of the authors' knowledge, the application of BISMC, RBFNN, and NDO in the context of FJR systems with hydraulic actuators is novel. RBF neural networks are designed to address unknown nonlinear functions, and disturbance observers are introduced to compensate for the influence of variable stiffness, disturbances, and the approximation error caused by NN. Consequently, the proposed controller can eliminate unexpected impacts from complex unknown system dynamics and unknown bound disturbances, achieving high-accuracy tracking control simultaneously.
3. The stability of the closed-loop system is analyzed and verified using Lyapunov theory. The analysis demonstrates that all the variables are bounded, and tracking errors can enter a small region near the zero domain. Finally, simulation analysis and experimental results under various conditions are conducted to validate the effectiveness of the proposed controller.

The remainder of this paper is organized in the following. In Section 2, the modeling of FJR including actuator dynamics and some preliminaries, are presented. Section 3 of this paper gives an adaptive NN-based BISMC control approach for VSA with disturbance observer. Simulation and experiments are investigated in Section 4 to verify the effectiveness of the proposed controller. At the end of the paper, the conclusion discusses and highlights some needed areas for future research.

2 | SYSTEMS DESCRIPTION AND SOME PRELIMINARIES

2.1 | Dynamic of system without actuator dynamics

A flexible joint robot with the integration of an ASRA using linear springs is introduced, which provides simultaneous control of position and stiffness via hydraulic cylinder and the stiffness motor at the same joint, as shown in Figure 1. The ASRA is based on a bidirectional motion of the direct current (DC) motor to regulate the joint stiffness, whilst the output link is controlled by a hydraulic system, including a servo valve, a hydraulic pump, a cylinder, and measurement components.
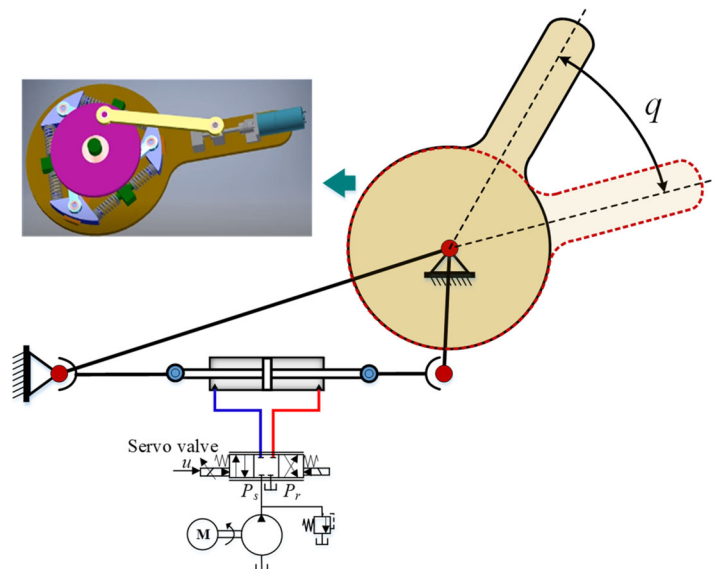

FIGURE 1 1-DOF flexible joint robot.

The dynamic system with load and gravity can be illustrated as follows:

$$\begin{cases} M_0 \ddot{q} + B_0 \dot{q} + G_0 + \tau_o = \tau_{ext} \\ M_1 \ddot{q}_1 + B_1 \dot{q}_1 - \tau_o = \tau_h \\ M_2 \ddot{q}_2 + B_2 \dot{q}_2 + \tau_k = \tau_m \end{cases} \tag{1}$$

where q, q_1, and q_2 denote the position of the output shaft, the positions of the principal cylinder, and stiffness motor; M_i ($i = 0, 1, 2$) describes the inertias of the output link, the position control cylinder, and stiffness control motor; G_0 is the gravity term; B_i presents the damping on the output link and relevant actuators (with gearbox and other transmission mechanisms); τ_m, τ_h is the control input torque supplied by stiffness and hydraulic actuator; τ_{ext} denotes the external torques on the output unit; τ_o, τ_k, in turn, are the spring elastic torque, and the resistant torque. $\theta = q - q_1$ describes the deflection angle between the output link and the immediate link.

The elastic torque τ_o can be determined as following[7,33]

$$\tau_o = \frac{\partial E}{\partial \theta} = -3K_s \left[\frac{2\gamma_3 Ra\left(L - \sqrt{R^2 - 2\gamma_1 Ra + a^2}\right)}{\sqrt{R^2 - 2\gamma_1 Ra + a^2}} + \frac{2\gamma_4 Ra\left(L - \sqrt{R^2 - 2\gamma_2 Ra + a^2}\right)}{\sqrt{R^2 - 2\gamma_2 Ra + a^2}} \right] = \Psi(q_1, q_2) \tag{2}$$

where E is the elastic potential energy in the spring; K_s is spring constant; $a, R, L, \gamma_i, (i = 1, 2, 3, 4)$, are the mechanical parameters of ASRA.

The stiffness K of the ASRA can be computed by the derivative of τ_o with respect to the deflection angle θ as follow:

$$K = \frac{\partial \tau_o}{\partial \theta} = f(q_2, \theta) \tag{3}$$

The resistant torque τ_k for the motor to regulate the stiffness is derived to be

$$\tau_k = \frac{b}{d.\eta.n}(F_1 \sin \alpha_1 - F_2 \sin \alpha_2) \tag{4}$$

where n is a ratio gearbox, and η is the ratio of the lead screw, b and d are the lengths of the long and short bars, F_i ($i = 1, 2$) is the internal force which generated by each of the springs, α_i defines the deflection angles between the applied force spring and the three-spoke element.

Remark 1. The details of mechanical design ASRA, that is, schematic model, prototype fabrication, are presented in a previous paper. The difference is only the pneumatic cylinder instead of the hydraulic cylinder. The interest-reader can research to further understand in Reference 7, In this article, the control strategy is investigated on the basic of the assuming about the knowledge of ASRA specifications.

Assumption 1. For the stiffness module, the controller inside the motor driver is sufficiently well such that the torque required by stiffness actuator τ_m can be accomplished by a linear function of input voltage u_2, for example, $\tau_m = k_m u_2$ where k_m is a positive constant.

2.2 | Hydraulic actuator dynamics

The dynamics of the pressures inside both chambers are formulated by

$$\dot{P}_L = \frac{4\beta_e}{V_c}(-A\dot{y} + Q_L - c_t P_L + Q_{Li}) \tag{5}$$

where C_t, V_c, and β_e are the coefficient of internal leakage, a fixed control volume of the cylinder, the Bulk modulus of hydraulic oil; A is an effective ram area. Q_{Li} is the time-varying deviation model including unmodeled pressure dynamics,

modeling error, etc. $P_L = P_1 - P_2$ defines the difference of pressure, P_1 and P_2 are the pressures inside the two chambers of the cylinder, respectively.

Assumed that the servo-valve dynamics is neglected, and the spool displacement of the servo valve is directly proportional to the control supplied. Thus, Q_L is load flow rate which is represented with respect to control input voltage by

$$Q_L = k_t u_1 \sqrt{P_s - sign(u_1)P_L} \tag{6}$$

where P_s is the supply pressure of the pump, k_t is a positive constant determined by the servo valve, u_1 is the control signal supplied by the controller, and *sign* is the signum function.

The hydraulic actuator is used to control the position of output link, which can be expressed by[34]

$$\dot{P}_L = -h_b P_L - h_c \dot{y} + u_1 h_a \sqrt{P_s - P_L sign(u_1)} + h_d Q_{Li} \tag{7}$$

where $h_a = \frac{4\beta_e k_t}{V_c}, h_b = \frac{4\beta_e C_0}{V_c}, h_c = \frac{4\beta_e A}{V_c}, h_d = \frac{h_a}{k_t}$.

The torque acting on joint is calculated by the

$$\tau_h = J^T A P_L \tag{8}$$

where J represents the differentiable actuator Jacobian matrix.

From the second equation of (1), one obtains τ_o and substituting it into the first equation of (1) yields

$$\ddot{q} = M_0^{-1}(-B_0\dot{q} - G_0) + M_0^{-1}J^T A P_L + M_0^{-1}(\tau_{ext} - M_1\ddot{q}_1 - B_1\dot{q}_1) \tag{9}$$

2.3 | The FJR dynamics including hydraulic actuator dynamics

Defining the FJR system state $x = \begin{bmatrix} q & \dot{q} & P_L & q_2 & \dot{q}_2 \end{bmatrix}^T = \begin{bmatrix} x_1 & x_2 & x_3 & x_4 & x_5 \end{bmatrix}^T$, and considering hydraulic actuator uncertainties, external disturbances, and nonlinearities resulted from the variable stiffness, the total system dynamics can be re-expressed as

$$\begin{cases} \dot{x}_1 = x_2 \\ \dot{x}_2 = f_1(x_2) + g_1 x_3 + d_1 \\ \dot{x}_3 = f_2(x_2, x_3) + g_2(x_3, u_1)u_1 + d_2 \\ \dot{x}_4 = x_5 \\ \dot{x}_5 = f_3(x_4, x_5) + g_3 u_2 \end{cases} \tag{10}$$

where $f_1 = M_0^{-1}(-B_0 x_2 - G_0); g_1 = M_0^{-1}J^T A; d_1 = M_0^{-1}(\tau_{ext} - M_1\ddot{q}_1 - B_1\dot{q}_1); f_2 = -h_c J x_2 - h_b x_3; d_2 = h_d Q_{Li} - h_c J\dot{\theta}. g_2 = h_a\sqrt{P_s - x_3 sign(u_1)}; f_3 = M_2^{-1}(-\tau_k - B_2 x_5); g_3 = k_m M_2^{-1}$.

Assumption 2. The lumped disturbances d_1, d_2, and their derivative are assumed to be smooth enough for model-based controller design and bounded, for example, $|d_1| \le d_{1m}, |d_2| \le d_{2m}, |\dot{d}_1| \le \delta_1, |\dot{d}_2| \le \delta_2$ where $d_{1m}, d_{2m}, \delta_1, \delta_2$ are positive constants.

Remark 2. The system dynamic can be divided into two parts: the output position of the ASRA is determined by the hydraulic actuator, and the stiffness of the ASRA is determined by the DC motor. The position and stiffness can be adjusted independently as Figure 2. The goal of the paper is to synthesize the control law (u_1, u_2) based on the NN and NDO that drive the output (q, K) tracking the desired trajectory (q_d, K_d) despite the unknown nonlinear uncertainty, disturbance and guarantee the stability of the whole closed-loop system.
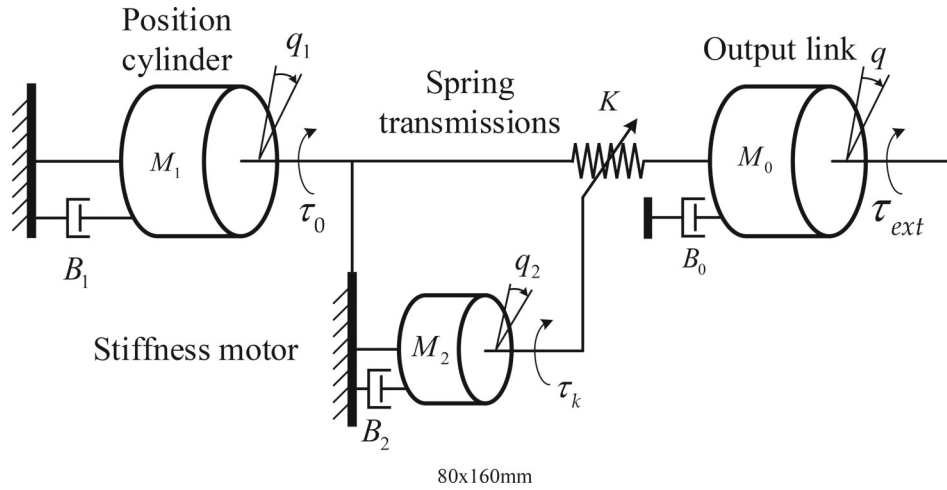
FIGURE 2 Schematic diagram of ASRA system.

3 | CONTROL SCHEME DESIGN

Considering the position control loop described by (10), an adaptive neural network backstepping integral sliding mode control with NDO is designed for FJR to achieve the high-precision tracking control, robustness property in the presence of uncertainty, and the impacts caused by nonlinearity of the variant stiffness actuation. Firstly, a model-based controller is built on the premise of the BISMC approach. Herein, we suppose that the information of the ASRA system is sufficiently provided. Next, the RBFNNs are utilized to approximate the unknown function for the case that components of the dynamic model are unavailable. Then, the NDO is constructed to compensate for the lumped disturbance, including the influence of the variable stiffness, various uncertainties of the hydraulic servo system, and the approximation error caused by NN. Finally, the stability of the closed-loop systems is rigorously analyzed based on the Lyapunov synthesis approach.

3.1 | Model-based controller

We define a series of the tracking error variables e_i as follows

$$e_i = x_i - x_{id}; i = 1 \div 3 \tag{11}$$

where x_{1d} is the desired position. Hence, let chosen the virtual control x_{2d}

$$x_{2d} = -k_1 e_1 + \dot{x}_{1d}, \quad k_1 > 0 \tag{12}$$

The derivative of e_2 is defined as the following:

$$\dot{e}_2 = f_1 + g_1 x_3 + d_1 - \dot{x}_{2d} \tag{13}$$

To control the e_2 to be as small as possible in case of the knowledge of d_1, the virtual control x_{3d} can be given by:

$$x_{3d} = \frac{1}{g_1}(-f_1 + \dot{x}_{2d} - e_1 - k_2 e_2 - d_1) \tag{14}$$

Defining the sliding surface with integral term as follow

$$s = e_3 + \beta e_2 + \vartheta \int_0^t e_2(\varsigma)d\varsigma, \forall t \geq 0 \tag{15}$$

where β, ϑ is a positive definite.

The derivative of the sliding variable s, is expressed as

$$\dot{s} = \dot{e}_3 + \beta \dot{e}_2 + \vartheta e_2 = f_2 + g_2 u_1 + d_2 - \dot{x}_{3d} + \beta \dot{e}_2 + \vartheta e_2 \tag{16}$$

The final law control is constructed to eliminate the influence caused by the variable stiffness, disturbance whilst ensuring the system stability and output link tracking position with small error.

To get the final law control, a fast sliding mode-type reaching phase,[35,36] is chosen:

$$\dot{s} + \psi s + \lambda sign(s) = 0 \tag{17}$$

where ψ, λ are two positive constants for the reaching phase.

If d_2 is known, the final control input can be expressed as the sum of two terms as follows:

$$u_1 = u_a + u_r \tag{18}$$

where the equivalent control law is chosen using the nominal plant parameters and constructed as

$$u_a = \frac{1}{g_2}(-f_2 + \dot{x}_{3d} - g_1 e_2 - \beta \dot{e}_2 - \vartheta e_2 - d_2) \tag{19}$$

and the switch control law is designed to deal with the matched disturbance and given by

$$u_r = \frac{1}{g_2}(-\psi s - \lambda sign(s)) \tag{20}$$

3.2 | System dynamics estimation using RBFNN

However, for a practical robotic system with variable stiffness joints, there exist values that are difficult to achieve accuracy, for instance, the unknown nonlinear dynamic function f_1, f_2. Hence, the model-based controllers cannot be given. Hence, RBFNNs are employed to approximate these unknown functions as

$$f_i = W_i^{*T} h_i + \varepsilon_i; i = 1 \div 2 \tag{21}$$

where $W_i^*, h_i, \varepsilon_i$ are the ideal weight, Gaussian function, and the approximate error.

$$h_i(x_{in}) = e^{-\frac{\|x_{in} - \omega_j\|^2}{2b_j^2}} \tag{22}$$

where x_{in} denotes the input vector of NN, $j = 1 \div N$, N is the number of the basic functions; ω_j and b_j are the center and width of the Gaussian function.

The estimated value of f_i can be calculated by

$$\begin{aligned} \widehat{f}_i &= \widehat{W}_i^T h_i \\ \tilde{f}_i &= f_i - \widehat{f}_i = \tilde{W}_i^T h_i + \varepsilon_i, \end{aligned} \tag{23}$$

where $\tilde{f}_i$, $\tilde{W}_i$, and $\widehat{W}_i$ are, in turn, the approximation error of nonlinear function f_i, the weight estimation error, and the estimated value of the ideal weight of the RBFNN.

To increase the robustness of the RBFNN, the adaptive law of weight value is determined as

$$\begin{aligned} \dot{\widehat{W}}_1 &= \Gamma_1^{-1}\left(h_1 e_2 - \lambda_1 \widehat{W}_1\right) \\ \dot{\widehat{W}}_2 &= \Gamma_2^{-1}\left(h_2 s - \lambda_2 \widehat{W}_2\right) \end{aligned} \tag{24}$$

where Γ_i, λ_i $(i = 1,2)$ are positive constants of the adaptive estimation law.

Assumption 3. The approximation error and weight value of the RBFNN are bounded as $\varepsilon_i < \varepsilon_N$, $\|W_i\|_F < W_M$ where ε_N and W_M are positive constants.

Remark 3. Although g_1 and g_2 share some parameters with the respective unknown nonlinear terms f_1 and f_2, we can achieve some preliminary information for the parameters of function g_1 and g_2 when an actuator is equipped for a practical system. Additionally, the perfect model of nonlinear control input terms g_1 and g_2 are available to facilitate the control design procedure.

3.3 | Control design using RBFNN and NDO

In (14), (19), if the disturbance d_1, d_2 are known, then the control law can be directly applied to the plant. Nonetheless, both d_1 and d_2 are unknown in practical application. Hence, the nonlinear disturbance observer can be elaborated which depends on the achieved information from NN approximator and shown as,[17,37]

$$\dot{\hat{z}}_a = -L_1\hat{z}_a + e_2 + L_1\left(-\hat{f}_1 - g_1x_3 - p_a\right)$$
$$\hat{d}_1 = \hat{z}_a + p_a$$

(25)

where $\hat{d}_1$ is the estimation value of the disturbance d_1, $\hat{z}_a$ is the internal states of the NDO.

The designed function p_a is selected as follow:

$$p_a = c_1x_2$$

(26)

where c_1 is a positive constant.

And the NDO gain L_1 is determined by the following.

$$L_1 = \frac{\partial p_a}{\partial x_2}$$

(27)

The estimated disturbance of d_1 and the approximation of f_1 are substituted to (14), then the actual x_{3d} can be re-expressed by

$$\hat{x}_{3d} = \frac{1}{g_1}\left(-\hat{f}_1 + \dot{x}_{2d} - e_1 - k_2e_2 - \hat{d}_1\right)$$

(28)

Similarly, the NDO to estimate d_2 is given by

$$\dot{\hat{z}}_b = -L_2\hat{z}_b + s + L_2\left(-\hat{f}_2 - g_2u_1 - p_b\right)$$
$$\hat{d}_2 = \hat{z}_b + p_b$$

(29)

where $p_b = c_2x_3$; $L_2 = c_2$ is positive constant. $\hat{d}_2$ is the estimation value of the disturbance d_2; $\hat{z}_b$ is the internal states of the NDO.

Then, the following final control law is redesigned:

$$u_1 = \frac{1}{g_2}\left(-\hat{f}_2 + \dot{\hat{x}}_{3d} - (g_1 + \vartheta)e_2 - \beta\dot{e}_2 - \hat{d}_2 - \psi s - \lambda sign(s)\right)$$

(30)

Define the observer error $\tilde{d}_i = d_i - \hat{d}_i (i = 1 \div 2)$.

It follows from (25 to 29) that the derivative of observer errors are given by

$$\dot{\tilde{d}}_1 = \dot{d}_1 - \dot{\hat{d}}_1 = \dot{d}_1 - L_1\tilde{d}_1 - e_2 - L_1\tilde{f}_1$$
$$\dot{\tilde{d}}_2 = \dot{d}_2 - \dot{\hat{d}}_2 = \dot{d}_2 - L_2\tilde{d}_2 - s - L_2\tilde{f}_2$$
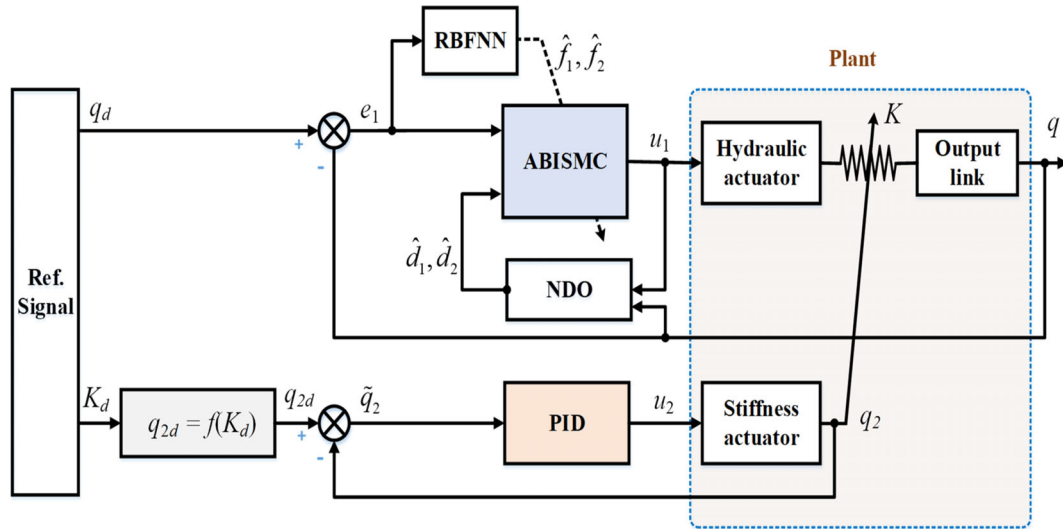
(31)

FIGURE 3   Diagram of proposed controller.

The block diagram of the control scheme is depicted in Figure 3. The control system comprises two modules: the proposed controller, designed to regulate the output position of the ASRA by controlling the hydraulic actuator, and the PID controller, which is applied to adjust the stiffness of the ASRA by controlling the DC motor. It is important to note that there is an interaction between these two components, posing challenges for the control problem. To address these challenges, the impact of variant stiffness is integrated into lumped disturbances, denoted as d_1 and d_2. To mitigate the effects of the interaction between stiffness control and output position control, the NDO is employed to estimate the lumped disturbances. This estimation allows for feed-forward compensation, diminishing the impact during controller design. The proposed controller is synthesized based on the ABISMC, RBFNN, and NDO, aiming to drive the output q to track the desired trajectory q_d under unknown system dynamics and lumped disturbances. Simultaneously, the PID controller ensures that the output stiffness K effectively tracks the reference signal K_d.

Theorem 1. For the ASRA model including hydraulic actuator (10), if the integral sliding manifold is selected as (15), the control law is (30), the adaptive law of weight value is defined as (24), the NDO is provided by (25), (29), then all the variables of the closed loop system are bounded.

Remark 4. Compared with previous works,[29–31] the FJR system considered in this study eliminates the assumption that the system dynamics are known. Instead, the lumped disturbance, including the influence of variable stiffness and external disturbances, is observed by an NDO, enhancing the feasibility of the FJR system. Compared with previous works,[23–26,32,33] the unknown nonlinear function is approximated by the NNs, and the presented observer is only considered the external disturbance. However, the the approximation error caused by NN and the impacts of variable stiffness are neglected.

Remark 5. To alleviate the chattering phenomenon, the *sign*(·) function is replaced by the saturation function $sat(\cdot)$ in (30) as[34]

$$sat\left(\frac{s}{\varsigma}\right) = \begin{cases} sign(s) & \text{if } |s| \geq \varsigma \\ \frac{s}{\varsigma} & \text{otherwise} \end{cases} \tag{32}$$

where ς is a small and positive constant.

3.4 | Stability analysis

By considering the impact of $\tilde{d}_1$, $\tilde{W}_1$ to the system's stability, the Lyapunov function candidate V_1 is selected as

$$V_1 = \frac{1}{2}e_1^2 + \frac{1}{2}e_2^2 + \frac{1}{2}\tilde{d}_1^2 + \frac{1}{2}\tilde{W}_1^T\Gamma_1\tilde{W}_1 \tag{33}$$

Differentiating (33) with respect to time and using (24), (31), the $\dot{V}_1$ is given by

$$
\begin{aligned}
\dot{V}_1 &= e_1(e_2 - k_1 e_1) + e_2(\tilde{f}_1 + \tilde{d}_1 - k_2 e_2 + g_1 e_3 - e_1) + \tilde{d}_1(\dot{d}_1 - L_1\tilde{d}_1 - e_2 - L_1\tilde{f}_1) - \tilde{W}_1^T\Gamma_1\widehat{\dot{W}}_1 \\
&= -k_1 e_1^2 - k_2 e_2^2 - L_1\tilde{d}_1^2 + e_2\varepsilon_1 + g_1 e_2 e_3 - L_1\tilde{d}_1\tilde{f}_1 + \tilde{d}_1\dot{d}_1 + \lambda_1\tilde{W}_1^T\widehat{W}_1
\end{aligned}
\tag{34}
$$

To analyze the stability of overall system, we consider the following Lyapunov function candidate:

$$
V_2 = V_1 + \frac{1}{2}s^2 + \frac{1}{2}\tilde{d}_2^2 + \frac{1}{2}\tilde{W}_2^T\Gamma_2\tilde{W}_2
\tag{35}
$$

Taking the derivative of Lyapunov function (35) with respect to time, and following (24), (31), (34), one obtains:

$$
\dot{V}_2 = -k_1 e_1^2 - k_2 e_2^2 - \psi s^2 - g_1\beta e_2^2 - \lambda|s| - \sum_{i=1}^{2}L_i\tilde{d}_i^2 + \sum_{i=1}^{2}\lambda_i\tilde{W}_i^T\widehat{W}_i + \sum_{i=1}^{2}\left(-L_i\tilde{d}_i\tilde{f}_i + \tilde{d}_i\dot{d}_i\right) + e_2\varepsilon_1 + s\varepsilon_2
\tag{36}
$$

It is noted that.

$$
\sum_{i=1}^{2}\lambda_i\tilde{W}_i^T\widehat{W}_i = \sum_{i=1}^{2}\lambda_i\tilde{W}_i^T\left(W_i^* - \tilde{W}_i\right) = \sum_{i=1}^{2}\left(-\lambda_i\tilde{W}_i^T\tilde{W}_i + \lambda_i\tilde{W}_i^T W_i^*\right) \text{ and } -L_i\tilde{d}_i\tilde{f}_i = -L_i\tilde{d}_i\left(\tilde{W}_i^T h_i + \varepsilon_i\right).
$$

Using Young's inequality, we have

$$
\begin{aligned}
\sum_{i=1}^{2}\lambda_i\tilde{W}_i^T\widehat{W}_i &\leq \sum_{i=1}^{2}\left(-\tfrac{\lambda_i}{2}\|\tilde{W}_i\|^2 + \tfrac{\lambda_i}{2}\|W_i^*\|^2\right) \\
-L_i\tilde{d}_i\tilde{W}_i^T h_i &\leq \tfrac{L_i}{2}\left(\chi_i\tilde{d}_i\right)^2 + \tfrac{L_i}{2}\|\tilde{W}_i\|^2 \\
-L_i\tilde{d}_i\varepsilon_i &\leq \tfrac{L_i}{2}\tilde{d}_i^2 + \tfrac{L_i}{2}\|\varepsilon_i\|^2
\end{aligned}
\tag{37}
$$

where $\|h_i\| \leq \chi_i, i = 1, 2$, χ_i are positive constants.

Similarly, consider the following inequalities:

$$
\begin{aligned}
\tilde{d}_i\dot{d}_i &\leq \tfrac{1}{2}\left(\tilde{d}_i\right)^2 + \tfrac{1}{2}\delta_i^2, i = 1, 2; \\
e_2\varepsilon_1 &\leq \tfrac{1}{2}e_2^2 + \tfrac{1}{2}\varepsilon_1^2; \\
s\varepsilon_2 &\leq \tfrac{1}{2}s^2 + \tfrac{1}{2}\varepsilon_2^2;
\end{aligned}
\tag{38}
$$

From (37), (38) and Assumption 2, 3, we obtain

$$
\begin{aligned}
\dot{V}_2 \leq &-k_1 e_1^2 - \left(k_2 - \tfrac{1}{2}\right)e_2^2 - \left(\psi - \tfrac{1}{2}\right)s^2 - \sum_{i=1}^{2}L_i\left(\tfrac{1}{2} - \tfrac{1}{2L_i} - \tfrac{\chi_i^2}{2}\right)\tilde{d}_i^2 - \frac{(\lambda_i - L_i)}{2}\sum_{i=1}^{2}\|\tilde{W}_i\|^2 \\
&+ \tfrac{1}{2}\left(\sum_{i=1}^{2}(L_i + 1)\varepsilon_i^2 + \sum_{i=1}^{2}\lambda_i\|W_i^*\|^2 + \delta_i^2\right)
\end{aligned}
\tag{39}
$$

Denote $\kappa = \min\left(2k_1, 2k_2 - 1, 2\psi - 1, L_1\left(1 - \tfrac{1}{L_1} - \chi_1^2\right), L_2\left(1 - \tfrac{1}{L_2} - \chi_2^2\right), \lambda_1 - L_1, \lambda_2 - L_2\right)$ and $\xi = \tfrac{1}{2}\left(\sum_{i=1}^{2}(L_i + 1)\varepsilon_i^2 + \sum_{i=1}^{2}\lambda_i\|W_i^*\|^2 + \delta_i^2\right)$.

Then the derivative of V_2 can be re-expressed as

$$
\dot{V}_2 \leq -\kappa V_2 + \xi
\tag{40}
$$

From (40), one has:

$$
V_2 \leq \frac{\xi}{\kappa}\left(1 - e^{-\kappa t}\right) + V_2(0)e^{-\kappa t}
\tag{41}
$$

It is clear from (41) we have $\lim_{t\to\infty} V_2 = \xi/\kappa$, which means the Lyapunov function V_2 in (35) is convergent.[38] Hence, the closed-loop system signals $\tilde{d}_1, \tilde{d}_2, e_1, e_2, s$ are bounded. As the results, Theorem 1 is verified.

4 | NUMERICAL SIMULATION AND EXPERIMENT

4.1 | Simulation

To demonstrate the effectiveness of the proposed controller, simulation results are provided using Matlab/Simulink environment. The sampling time is selected as 0.5 ms. The simulation parameters of ASRA and the hydraulic actuator are listed as follows:

The ASRA parameter is set as[7]: $M_0 = 0.0153$ (kgm^2); $B_0 = 0.007$ (Nms/rad); $G_0 = 0$; $M_1 = 0.0284$ (kgm^2); $B_1 = 0.008$(Nms/rad); $M_2 = 0.019$ (kgm^2); $B_2 = 0.003$(Nms/rad); $\tau_{ext} = 1.5\sin(t)$. Other specifications of the stiffness module are defined as: $K_s = 4650$ N/m, $r = 25$ mm, $d_0 = 230$ mm, $d_{l1} = 100$ mm, $d_{l2} = 300$ mm, $l = 10$ mm, $L = 40$ mm, $R = 40$ mm, $\eta = 2$ mm, $n = 35{:}1$, $a = 56.5$ mm, $b = 130$ mm, $d = 52$ mm, $c = 25$ mm.

The system parameters of hydraulic actuator are set as[34]: $A = 0.0008042$ m^2; $P_s = 16$ Mbar; $h_a = 1.6 \times 10^5$ N $^{1/2}$(s·m^3); $h_b = 50$ (1/s); $h_c = 2 \times 10^{-7}$ (N/m^2); $k_t = 3.2 \times 10^{-8}$ (m^3/s/V/Pa$^{-1/2}$).

In this paper, the following three controllers are introduced for the position tracking problem to compare the performance of the proposed controller: integral sliding mode controller (ISMC), backstepping integral sliding mode control using NN (BISMCNN), and BISMCNN with NDO (proposed controller). Meanwhile, the PID controller is applied to regulate the stiffness of ASRA that is expressed as

$$u_2 = K_p \tilde{q}_2 + K_d \dot{\tilde{q}}_2 + K_i \int_0^t \tilde{q}_2(\tau) d\tau \tag{42}$$

where $K_p = 1.2$, $K_i = 0.02$, and $K_d = 0.75$ are, in turn, the proportional gain, the integral gain, and the derivative gain. $\tilde{q}_2 = q_2 - q_{2d}$ denotes the position error of the stiffness motor.

1. An ISMC[7] is selected as a baseline controller without considering the actuator dynamics. The control law of ISMC is given by:

$$u_1 = K_{1c}^{-1} \left[q_d + \lambda_{11}^{-1} \dot{e}_1 + \rho_{11}\sigma_1 + \rho_{12}sign(\sigma_1) \right] \tag{43}$$

where $K_{1c} = 1.5$, $\lambda_{11} = 5$, $\rho_{11} = 10$, and $\rho_{12} = 20$; and σ_1 is the sliding surface of the ISMC that is defined:

$$\sigma_1 = e_1 + \lambda_{11} \int_0^t e_1(\chi) d\chi \tag{44}$$

2. The gain parameters of the proposed controller are set as $k_1 = 100$; $k_2 = 100$; $\beta = 10$; $\vartheta = 5$; $\psi = 200$; $\lambda = 100$; and the NDO parameters are $L_a = 0.5$; $L_b = 10$. The NNs for f_1, f_2 approximation are defined 2-9-1; 3-21-1 corresponding the layer input-hidden-output, respectively. The parameters of NNs for f_1: $x_{in1} = [x_1 \ x_2]^T$ with the input range $[-20, 20] \times [-20, 20]$; $b_j = 2.5$. The centre ω_{i1} of the NN nodes are evenly spaced between the upper and lower bounds of the input range limits of ASRA joint. Thus, ω_{i1} is designed as $c_{i1} = [-25 + 5i_1; -25 + 5i_1]$, $i_1 = 1 \div 9$. The parameters of NNs for f_2: $x_{in2} = [x_1 \ x_2 \ x_3]^T$ with the range input $[-20, 20] \times [-20, 20] \times [-1000, 1000]$; $b_j = 3000$; and ω_{i2} is designed as $c_{if1} = [-25 + 5i_2; -25 + 5i_2; -1100 + 100i_2]$, $i_2 = 1 \div 21$.

   The initial weight value is chosen as zeros. The parameter adaption rates are chosen as $\Gamma_1 = 10$; $\Gamma_2 = 50$; $\lambda_1 = 0.8$; $\lambda_2 = 100$

3. The BISMCNN contains the similar control algorithm with proposed controller except for the NDO. For fair comparison, all design parameters of the BISMCNN controller are set as same as the corresponding parameters of the suggested controller.

Remark 6. The selections of parameters are tuned through the trial-and-error procedure as well as the experience of the designer which not only achieves the good tracking performance but also assures the system stability.

In order to evaluate the effectiveness of the suggested controller, the following performance indexes are introduced:

1. The integral absolute error (IAE) is utilized as an index of measure of precision tracking, which can be expressed as $\sigma_e = \sqrt{\frac{1}{T}\int_0^T |e|^2 dt}$

2. The maximum absolute value of error during the last ten seconds is defined as $e_M = \max\limits_{0 \leq t \leq T}\{|e(t)|\}$ where T defines the total simulation time

To validate the performance of the aforementioned controller design, the following two case studies will be presented.
Case study 1:

The aim is to make the output position link track a desired sinusoidal trajectory $q_d(t) = 10 (1 - \cos(\pi t)) (1 - \exp(-t))$ deg. Simultaneously, the stiffness of ASRA reaches the desired stiffness which is the square wave pulse, with an amplitude 130 Nm/rad, pulse width 50%. The initial state of the joints $q(0) = 0$ and $K(0) = 150$ Nm/rad.

The motion trajectories and tracking error of the output link are illustrated in Figure 4. From Figure 4, it is obvious that the ISMC provides the worst tracking performance under the existing disturbance and unknown dynamic system. In the case of neglecting the actuator dynamics, the position tracking of the ISMC depends on the selection of the large gains and cannot be satisfied as compared to the controllers proposed in the literature. Owning to the RBFNN approximator, the influence of unmodeled dynamics is solved, then the BISMCNN gives better tracking performance in comparison with ISMC. Nevertheless, the convergence time and steady-state errors of these controllers are still big due to the lack of disturbance compensation. With the perfect combination of the BISMCNN and the assistant of the NDO, the proposed controller provides the best performance.

The estimation performance of NDOs is displayed in Figure 5 while Figure 6 exhibits the adaption neural network law of f_1 and f_2. From Figure 6, it is obvious that the weight vector of the RBFNNs converges to a small neighborhood of the origin. The unknown nonlinear function and lumped disturbance are successfully approximated with the assist of NN and NDO. Hence, the lumped disturbances/uncertainties are compensated by the suggested control law, and the tracking performance is significantly enhanced. The IAE is computed between the actual output and the desired signal to measure the accuracy of the comparative controllers, as shown in Table 1.
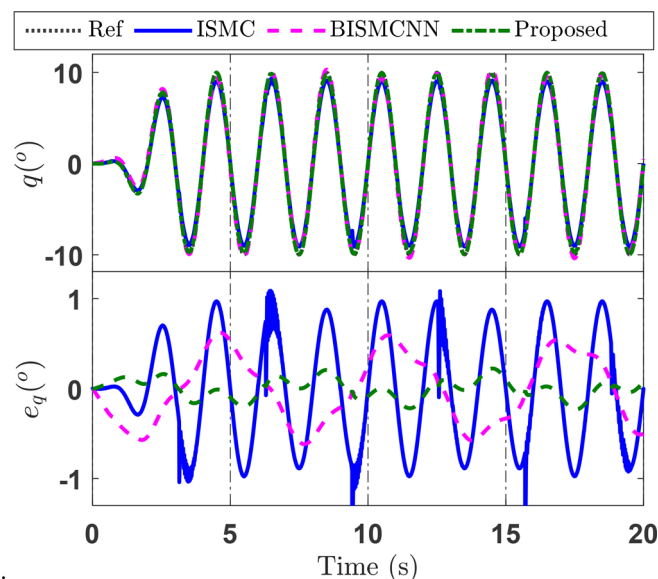

FIGURE 4 Position tracking performance of the comparative controllers case study 1.
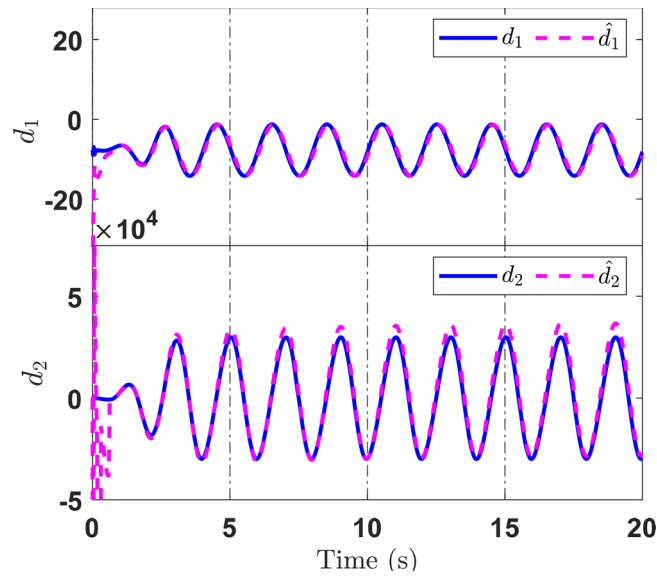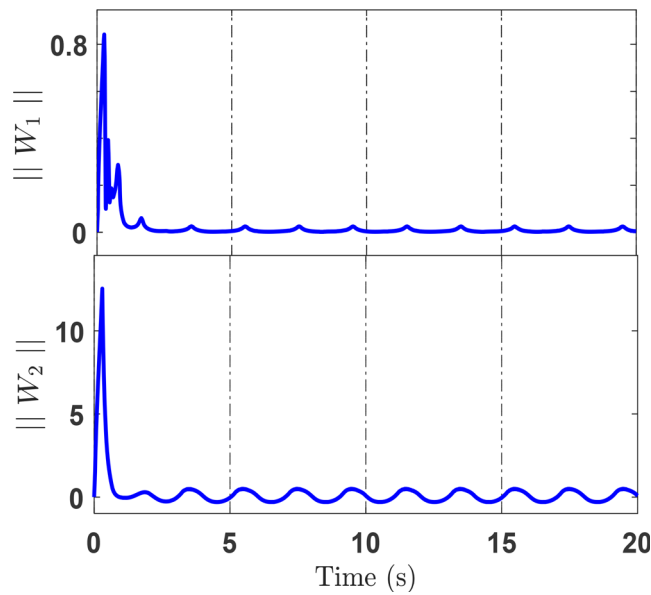
FIGURE 5 Disturbance estimation case study 1.

FIGURE 6 Norm of W_1 and W_2 case study 1.

TABLE 1 Performance indexes of three controllers in simulation.

	Controller	ISMC	BISMCNN	Proposed
Case study 1	σ_e	0.6242	0.5432	0.1116
	e_M	0.9733	0.6834	0.1776
Case study 2	σ_e	0.6806	0.3729	0.1024
	e_M	0.9510	0.4771	0.1094

The effects of the varying stiffness can be seen in Figure 7. The output elastic τ_0 and resistant torque τ_k show the fluctuation with respect to the stiffness adjustment. Although the output tracking suffers from the impacts of the variable stiffness, the performance of the suggested controller has still guaranteed small error thanks to the NDO.

For the stiffness module, the stiffness controller using the PID technique is designed. The control law u_2 in (42) drives the stiffness output following the desired trajectory. The stiffness tracking performance is shown in Figure 8. As seen Figure 8, the output stiffness tracks reference trajectory with small error thanks to PID controller. Although the stiffness and position output link can be independently regulated, the stiffness feature still has a meaningful role for different purposes. In the case of interacting with the environment, the stiffness will be lower to avoid the impact of the unwanted collision. On the other hand, the stiffness becomes stiffer when the requirement of the application is given, such as high accuracy position tracking, throwing a subject as far as possible, dismantling work, etc.
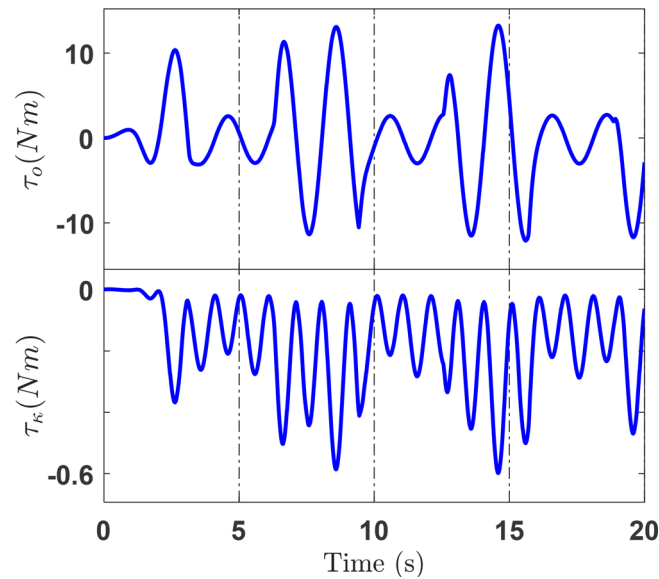
FIGURE 7 The output torque curve during both position and stiffness tracking case study 1.
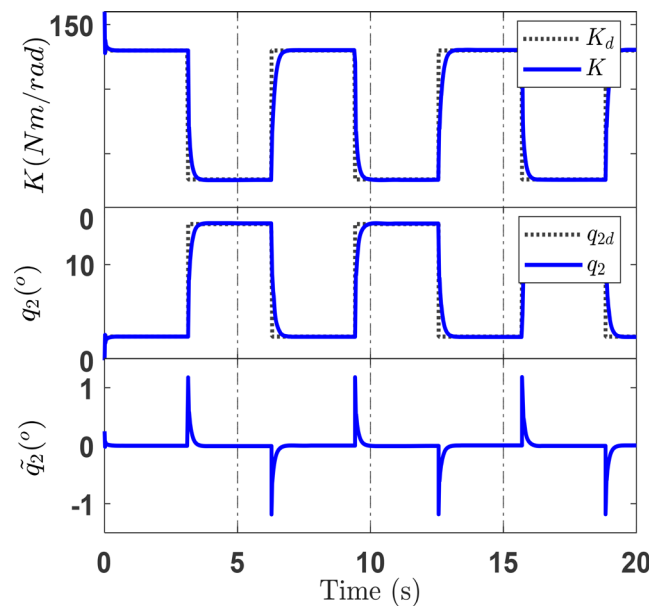

FIGURE 8 Stiffness tracking performance.

Case study 2:

To further validate the robustness of the proposed controller, the comparative controllers are then applied for multistep trajectory in which the tanh function is used to ensure the continuous features of a second-order derivable. The desired position can be described as

$$q_d(t) = \begin{cases} 5 - 5\tanh(100t) & \text{if } 0 \le t \le 2\text{s} \\ 5\tanh(100(t-2)) + 1 & \text{if } 2 < t \le 6\text{s} \\ 6 - 2\tanh(100(t-6)) & \text{if } 6 < t \le 10\text{s} \\ 10\tanh(100(t-10)) & \text{if } 10 < t \le 15\text{s} \\ 10 - 2\tanh(100(t-15)) & \text{if } 15 < t \le 20 \end{cases} \quad (\text{deg}) \quad (45)$$

The tracking performance of three controllers is depicted in Figure 9. It can be seen that the accuracy tracking of the proposed controller is better than the remaining controller in terms of tackling the effects of the disturbance/uncertainty. The performance indexes are shown in Table 1. Whilst the IAE of ISMC, BISMCNN are, in turn, 0.6806, 0.3729, the IAE of the proposed controller is only 0.1024 which improves the efficiency 85% and 72.5%, respectively. The comparison results between the BISMCNN and the proposed controller also indicate that the compensation of the NDO significantly degrades the effects of the disturbance on the system.

The convergence of the estimation result of the NDO is displayed in Figure 10, which shows the validity of the NDO. The employment of the NN to approximate unknown dynamics is able to overcome the requirement of an exact dynamic model. Figure 11 represents the boundedness of estimated parameters that provides the approximation value of the unknown components in the system dynamics so that the good performance of the proposed can be obtained. In addition, the internal torque, including elastic torque and resistant torque is generated during the motion system that is exhibited in Figure 12.

4.2 | Experiment

The hybrid nonlinear control approach was demonstrated on a real-time system through various experiments. The experimental test-rig of ASRA accounting for actuator dynamics is set up as shown in Figure 13. This testing system consists of the proposed ASRA and a control-data acquisition system, including a personal computer, a data acquisition (DAQ)
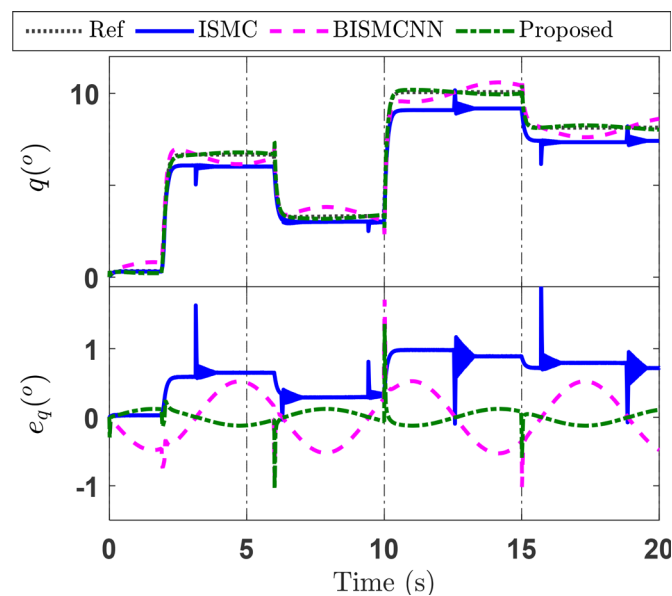

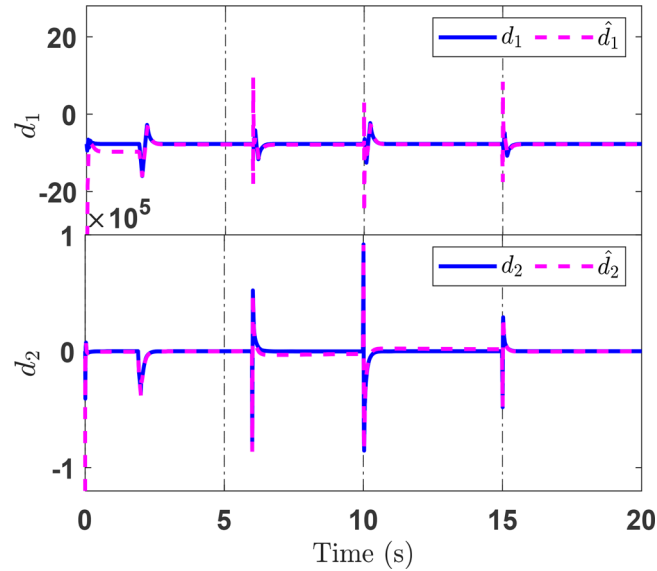**FIGURE 9** Position tracking performance of the comparative controllers case study 2.

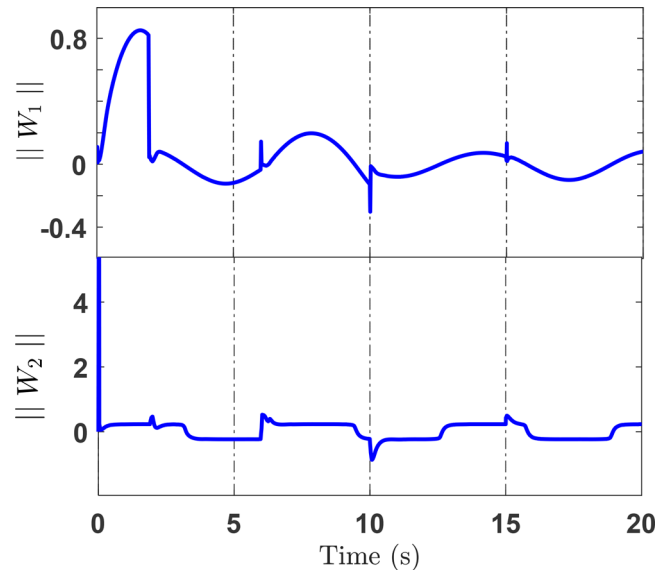**FIGURE 10**   Disturbance estimation case study 2.

FIGURE 11   Norm of W_1 and W_2 case study 2.

card (PCI-6014, Advantech), and the measurement system. Two transducer displacement and two pressure sensors were used to measure the output link position, the cylinder position, and the pressure inside of the EHA, respectively. Another part is the stiffness module which comprises of a DC motor (Maxon DCX26L-GB-KL-24 V with Gear ratio: 35:1) and an absolute encoder (Resolution: 4096 pulses/rev). Besides, the PCI-QUAD04 is deployed to provides inputs and decodes for two incremental quadrature encoders. The proposed controller was employed on the PC within the MATLAB/Simulink environment combined with the Real-time Window Target Toolbox. The setting parameters of the real system are listed in Table 2.

The main purpose of the experiments is to provide the practical applicability of the proposed control scheme for output link position tracking. The following scenarios are given as follow:

1. A sinewave trajectory with variable amplitude and frequency.
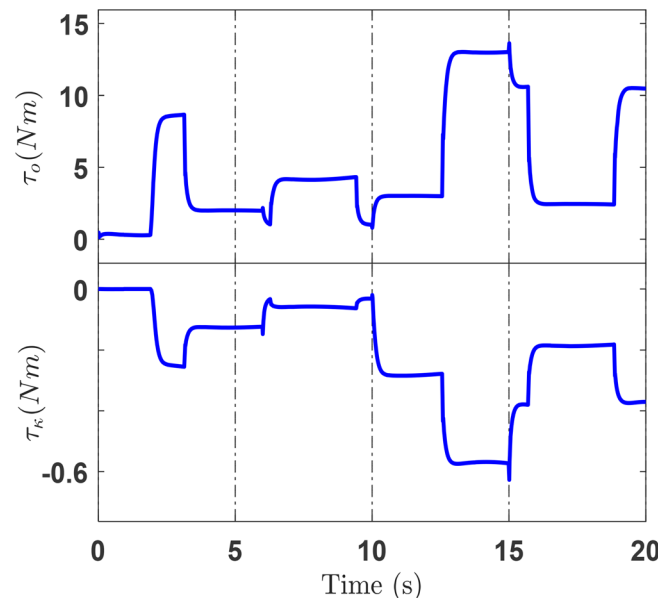2. A multistep trajectory.

FIGURE 12   The output torque curve during both position and stiffness tracking case study 2.
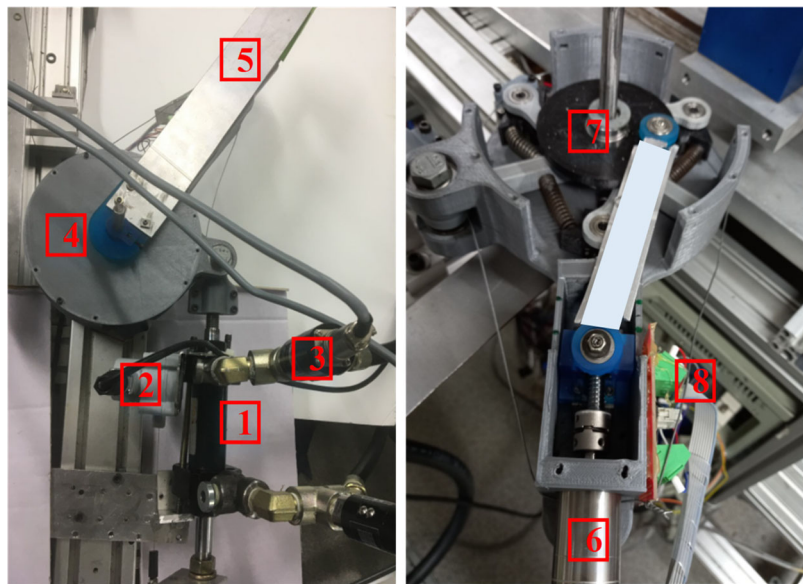

FIGURE 13   Output Single-link ASRA with the hydraulic actuator in experiment (1-a double rod cylinder, 2-wire sensor, 3-pressure sensor, 4-Stiffness module, 5-output link, 6-DC motor, 7-ASRA design, 8-Absolute encoder).

To show the influence of the adjustment stiffness, the opened-loop test is firstly conducted in which the stiffness value is set from $K = 10$ Nm/rad to $K = 130$ Nm/rad corresponding to "soft" and "stiff". Then, the control input u_1 is supplied to the valve, the output position link is recorded as displayed in Figure 14. It can be seen that the oscillation of the output link will decrease when the stiffness becomes stiffer.

Then, the closed-loop system is implemented with the employment of the different controllers to cope with the influence of the stiffness modulation, and various uncertainties of the hydraulic servo system. The two case studies are given as follow:

Case study 1: Considering the constraint of the stroke cylinder in the FJR system, the output tracking position demands are determined through coordinated transform as $q_d(t) = 10(1-\cos(\pi t))(1-\exp(-t))$ deg. As for the experiment, the parameters of ISMC controller in the Simulink are chosen as $K_{1c} = 4.5$, $\lambda_{11} = 15$, $\rho_{11} = 15$, and $\rho_{12} = 30$. In terms of the proposed

TABLE 2 Components setting of the real ASRA system.

| Module	Devices	Parameters	Specification
Position tracking	Hydraulic cylinder	Piston diameter	36 [mm]
		Rod diameter	12 [mm]
		Length of stroke	25 [mm]
	Servo valve	Model	MOOG—D633-317B
		Rated flow	10 [l/min]
	Pressure transducer	Pressure range	0–300 [bar]
		Rated output	30 [bar/V]
	Displacement sensor	Model	Rational WTB5-0500MM
		Full range	500 [mm]
	Rotary encoder	Type	E40H12-1024-3-V-5
		Resolution	4096 [pulses/rev]
	DAQ card	Model	NI PCI-6014
		Resolution	16AI/2AO: 16-bits
	PCI-QUAD04 (Quadrature encode input)	Number of channels	4
		Counter type	LS7266R1 24-bit
		I/O connector type	37-pin connector
Stiffness modulation	DC servo motor	Type	Maxon DCX26L-GB-KL
		Rated rotation speed	5060 [rpm]
		Gear ratio	35:1
		Absolute encoder	4096 [pulses/rev]
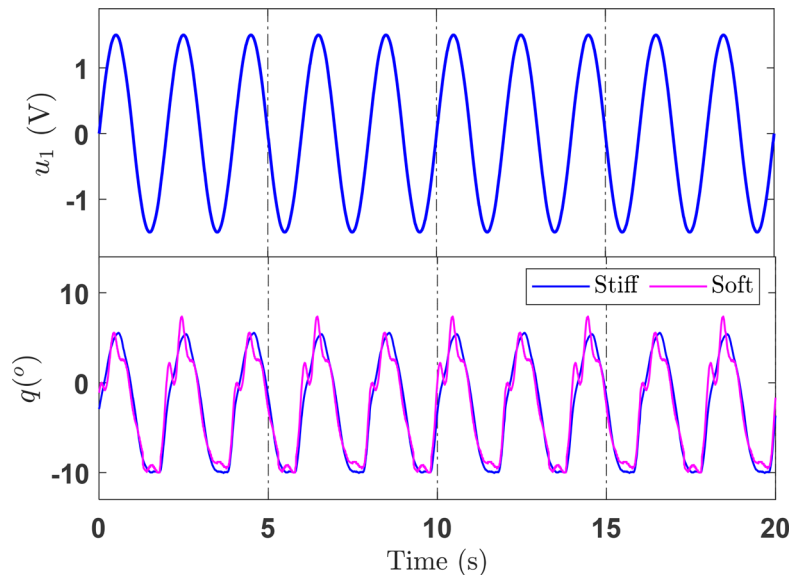
FIGURE 14 Output link q executed at 0.5 Hz when the stiffness at the transmission is constant with values $K = 10$ Nm/rad (soft) and $K = 130$ Nm/rad (stiff).

controller, the control gains and parameters are selected as $k_1 = 10; k_2 = 90; \beta = 10; \psi = 20; \lambda = 60; L_a = 25; L_b = 35; \Gamma_1 = 0.1; \Gamma_2 = 0.05; \lambda_1 = 8; \lambda_2 = 12$. The experiment results of this case are displayed in Figures 15–18. Figure 15 indicates that the position tracking errors of the suggested controller is smaller more than ISMC, and BISMCNN in the presence of unknown nonlinear dynamic uncertainties, disturbance. Because the unknown dynamic is approximated by the RBFNN, then it is compensated through the BISMCNN design, the tracking performance of BISMCNN is better than ISMC. However, due to the lack of disturbance compensation, the BISMCNN is still worse than the proposed controller. The estimation result of NDO is described in Figure 17 and the training process of NNs has been expressed via the bounded of the weight vector. Moreover, the performance indices are presented in Table 3. From Table 3, the (σ_e, e_M) deg of proposed controller is (0.0465, 0.1747) while the ISMC and BISMCNN have (0.2295, 0.6737) and (0.1249, 0.4830) deg. It again confirms the effectiveness of the suggested methodology in comparison with relevant controllers. Meanwhile, the stiffness of the joint can be independently adjusted by DC motor. The stiffness desired in the experiment is set as $K_d = 150 \sin(0.4\pi t)$ Nm/rad, and its performance tracking is displayed in Figure 16.
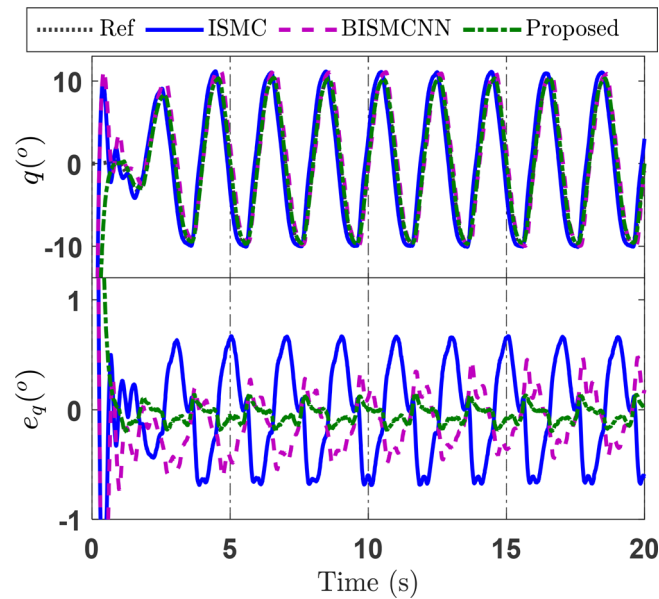

FIGURE 15   Position tracking performance of the comparative controllers case study 1 in experiment.
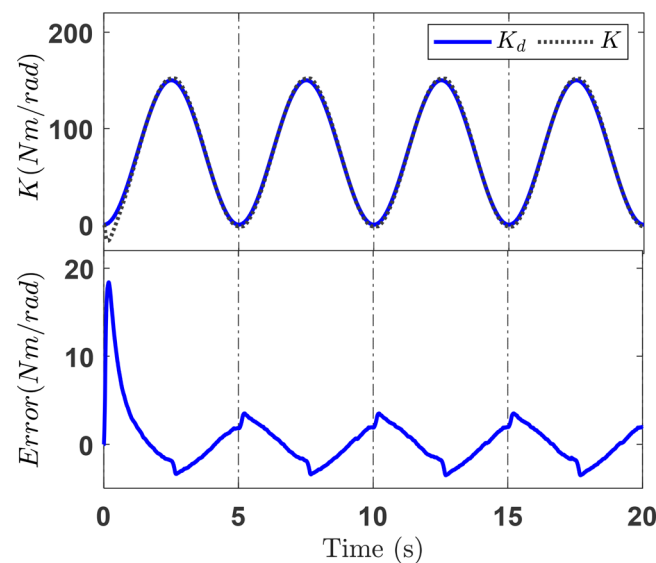

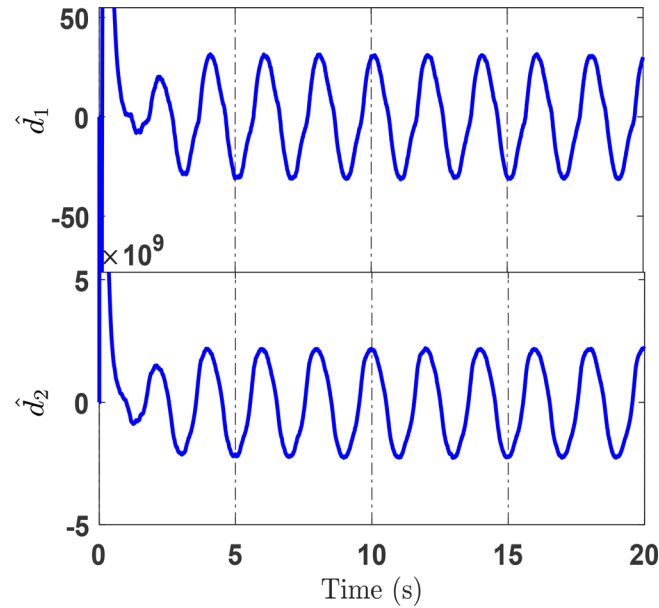**FIGURE 16**   Stiffness tracking performance in experiment.

FIGURE 17   Disturbance estimation case study 1 in experiment.
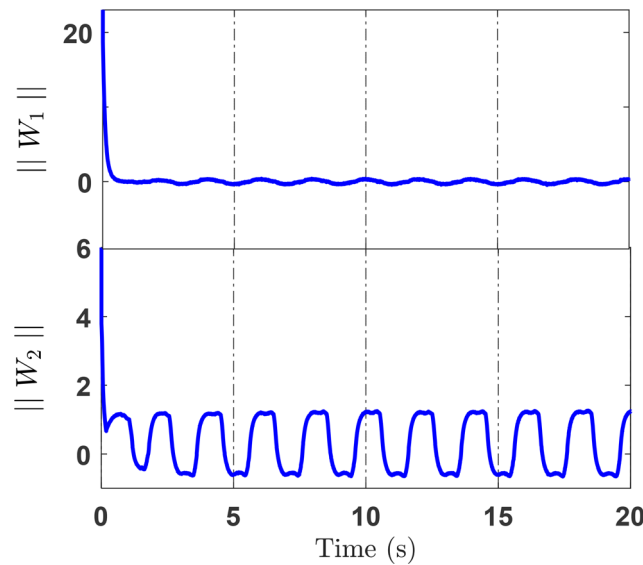

FIGURE 18   Norm of W_1 and W_2 case study 1 in experiment.

Case study 2: In this case study, the multistep reference in (45) is employed to further verify the effectiveness of the proposed control strategy. From Figure 19, it is clear that the ISMC and BISMCNN exhibit large tracking error with $\sigma_e = 0.0993$ deg, $e_M = 0.66$ deg and $\sigma_e = 0.0939$ deg, $e_M = 0.6522$ deg, respectively. BISMCNN gives slower tracking error than ISMC because two NNs are employed in BISMC approach. Meanwhile, owning to both the compensation of NDO and the impressive approximation ability of RBFNN, the suggested controller obtains superior tracking performance $\sigma_e = 0.079$ deg, $e_M = 0.6304$ deg without overshoot. The estimated value of d_1 and d_2 is depicted in Figure 20, these results provide for the controller to reject disturbances. Figure 21 shows the curves of the adaptive neural network approximation $\widehat{W}_1$ and $\widehat{W}_2$ by (32). It can be observed that the estimated parameters are bounded.

The results of simulation and experimental reveal that the tracking performance of the proposed controller for FJR with integration of an ASRA including actuator dynamic ensures high accuracy, less oscillation in the events of the changing of the stiffness, unknown nonlinear dynamics, and disturbances.

TABLE 3 Performance indexes of three controllers in experiment.

	Controller	ISMC	BISMCNN	Proposed
Case study 1	σ_e	0.2295	0.1249	0.0465
	e_M	0.6737	0.4830	0.1747
Case study 2	σ_e	0.0993	0.0939	0.0790
	e_M	0.6600	0.6522	0.6304
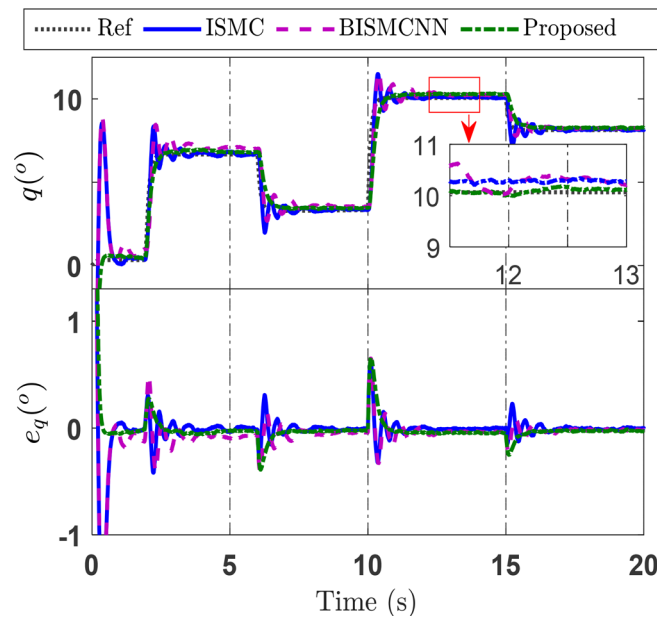
FIGURE 19 Position tracking performance of the comparative controllers case study 2 in experiment.
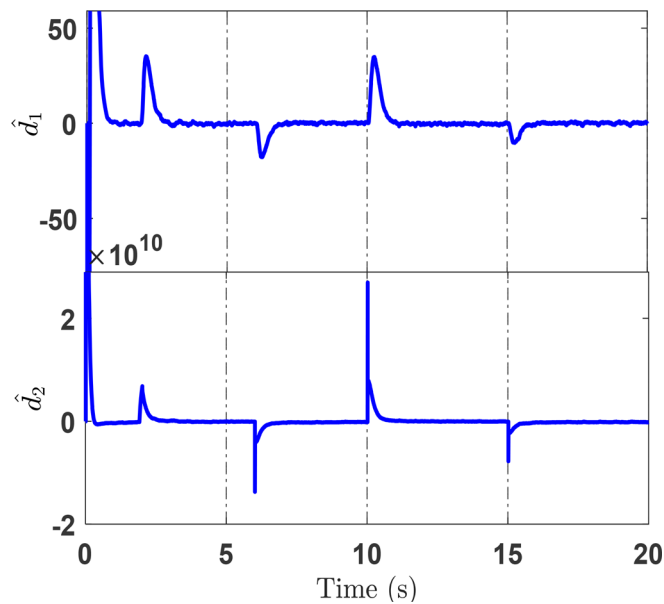

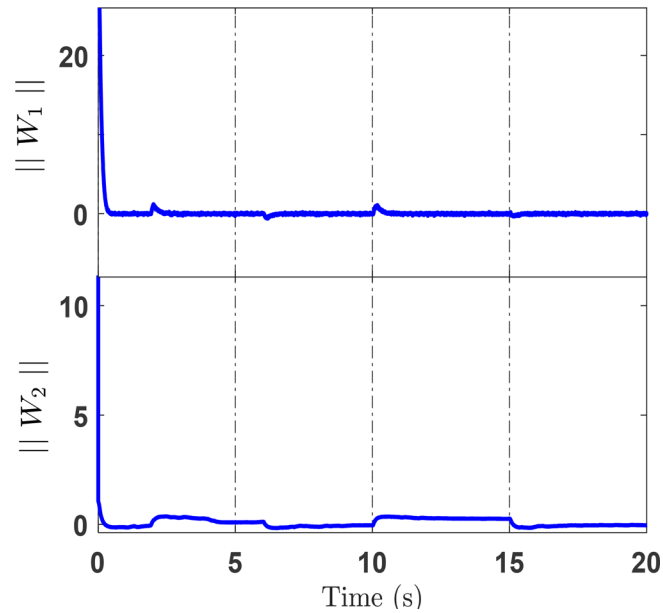**FIGURE 20** Disturbance estimation case study 2 in experiment.

FIGURE 21 Norm of W_1 and W_2 case study 2 in experiment.

5 | CONCLUSION

In this paper, the NDO-based BISMCNN has been proposed for FJR with the integration of an ASRA accounting for hydraulic actuator dynamics. Firstly, the NNs are designed to approximate the unknown function and the adaptive law for the NN weights are then derived. Next, the NDO was augmented to compensate for the lumped disturbances caused by the effects of variable stiffness, various uncertainties of the hydraulic servo system, as well as the approximation error of RBFNN. Finally, the integration of the BISMC and the above technique is developed to obtain satisfactory performance while the system stability has still been maintained in the presence of disturbance, model uncertainties, and the influence of the variable stiffness. The numerical simulation and experiment results are investigated to validate the effectiveness and feasibility of the suggested controller. In future research, the advanced controller applied for multi-flexible joint robots using ASRA will be studied.

CONFLICT OF INTEREST STATEMENT
The authors declare no conflict of interest.

DATA AVAILABILITY STATEMENT
Data sharing is not applicable to this article as no new data were created or analyzed in this study.

ORCID
Van Du Phan https://orcid.org/0000-0003-1380-5230
Cong Phat Vo https://orcid.org/0000-0001-6703-5759
Kyoung Kwan Ahn https://orcid.org/0000-0002-7927-3348

REFERENCES
1. Ham R, Sugar T, Vanderborght B, Hollander K, Lefeber D. Compliant actuator designs. *IEEE Robot Autom Mag*. 2009;16(3):81-94.
2. Mengacci R, Keppler M, Pfanne M, Bicchi A, Ott C. Elastic structure preserving control for compliant robots driven by agonistic-antagonistic actuators (ESPaa). *IEEE Robot Autom Lett*. 2021;6(2):879-886.

3. Choi H, Piao J, Kim ES, et al. Intuitive bilateral teleoperation of a cable-driven parallel robot controlled by a cable-driven parallel robot. *Int J Control Autom Syst*. 2020;18(7):1792-1805.

4. Lee HD, Moon JI, Kang TH. Design of a Series Elastic Tendon Actuator Based on gait analysis for a walking assistance exosuit. *Int J Control Autom Syst*. 2019;17(11):2940-2947.

5. Wolf S, Grioli G, Eiberger O, et al. Variable stiffness actuators: review on design and components. *IEEE/ASME Trans Mechatron*. 2016;21(5):2418-2430.

6. Sun J, Guo Z, Zhang Y, Xiao X, Tan J. A novel Design of Serial Variable Stiffness Actuator Based on an Archimedean spiral relocation mechanism. *IEEE/ASME Trans Mechatron*. 2018;23(5):2121-2131.

7. Vo CP, Phan VD, Nguyen TH, Ahn KK. A compact adjustable stiffness rotary actuator based on Linear Springs: working principle, design, and experimental verification. *Actuators*. 2020;9(4):141-156.

8. Ba K-x et al. A nonlinear model-based variable impedance parameters control for position-based impedance control system of hydraulic drive unit. *Int J Control Autom Syst*. 2020;18(7):1806-1817.

9. Thien TD, Ba DX, Ahn KK. Adaptive backstepping sliding mode control for equilibrium position tracking of an electrohydraulic elastic manipulator. *IEEE Trans Ind Electron*. 2020;67(5):3860-3869.

10. Guo Q, Chen Z. Neural adaptive control of single-rod electrohydraulic system with lumped uncertainty. *Mech Syst Signal Process*. 2021;146:106869-106885.

11. Phan VD, Vo CP, Dao HV, Ahn KK. Robust fault-tolerant control of an electro-hydraulic actuator with a novel nonlinear unknown input observer. *IEEE Access*. 2021;9:30750-30760.

12. Florian Petit AD, Albu-Schäffer A. Backstepping control of variable stiffness robots. *IEEE Trans Control Syst Technol*. 2015;23(6):2195-2202.

13. Sardellitti I, Medrano-Cerda GA, Tsagarakis N, Jafari A, Caldwell DG. Gain scheduling control for a class of variable stiffness actuators based on lever mechanisms. *IEEE Trans Robot*. 2013;29(3):791-798.

14. Melchiorri GPAC, Luca AD. On the feedback linearization of robots with variable joint stiffness. *2008 IEEE International Conference on Robotics and Automation*. IEEE; 2008;1753-1759.

15. Psomopoulou E, Theodorakopoulos A, Doulgeri Z, Rovithakis GA. Prescribed performance tracking of a variable stiffness actuated robot. *IEEE Trans Control Syst Technol*. 2015;23(5):1914-1926.

16. Yao J. Model-based nonlinear control of hydraulic servo systems: challenges, developments and perspectives. *Front Mech Eng*. 2017;13(2):179-210.

17. Zhang L, Li Z, Yang C. Adaptive neural network based variable stiffness control of uncertain robotic systems using disturbance observer. *IEEE Trans Ind Electron*. 2017;64(3):2236-2245.

18. Sun C, He W, Hong J. Neural network control of a flexible robotic manipulator using the lumped spring-Mass model. *IEEE Trans Syst Man Cybern Syst*. 2017;47(8):1863-1874.

19. Doukhi O, Lee DJ. Neural network-based robust adaptive certainty equivalent controller for quadrotor UAV with unknown disturbances. *Int J Control Autom Syst*. 2019;17(9):2365-2374.

20. He W, Ouyang Y, Hong J. Vibration control of a flexible robotic manipulator in the presence of input Deadzone. *IEEE Trans Ind Inform*. 2017;13(1):48-59.

21. Guo Z, Pan Y, Sun T, Zhang Y, Xiao X. Adaptive neural network control of serial variable stiffness actuators. *Complexity*. 2017;2017:5361246-5361254.

22. Sunghoi Huh GT, Bicchi A. Neural network based robust adaptive control for a variable stiffness actuator. Proceedings of the 16th Mediterranean Conference on Control and Automation. 2008 1028–1034.

23. Rahmani M, Rahman MH. Adaptive neural network fast fractional sliding mode control of a 7-DOF exoskeleton robot. *Int J Control Autom Syst*. 2019;18(1):124-133.

24. Ren H, Ma H, Li H, Wang Z. Adaptive fixed-time control of nonlinear MASs with actuator faults. *IEEE/CAA J Autom Sinica*. 2023;10(5):1252-1262.

25. Nguyen MN, Tran DT, Ahn KK. Robust position and vibration control of an electrohydraulic series elastic manipulator against disturbance generated by a variable stiffness actuator. *Mechatronics*. 2018;52:22-35.

26. Zaare S, Soltanpour MR. Adaptive fuzzy global coupled nonsingular fast terminal sliding mode control of n-rigid-link elastic-joint robot manipulators in presence of uncertainties. *Mech Syst Signal Process*. 2022;163:108165-108190.

27. Mohammadi A, Tavakoli M, Marquez HJ, Hashemzadeh F. Nonlinear disturbance observer design for robotic manipulators. *Control Eng Pract*. 2013;21(3):253-267.

28. Guo Z, Sun J, Ling J, Pan Y, Xiao X. Robust trajectory tracking control for variable stiffness actuators with model perturbations. *Front Neurorobot*. 2019;13:35-45.

29. Guo J, Guo J, Xiao Z. Robust tracking control for two classes of variable stiffness actuators based on linear extended state observer with estimation error compensation. *Int J Adv Robot Syst*. 2020;17(2):1-9.

30. Hua X, Huang D, Guo S. Extended state observer based on ADRC of linear system with incipient fault. *Int J Control Autom Syst*. 2019;18(6):1425-1434.

31. Serio A, Grioli G, Sardellitti I, Tsagarakis NG, Bicchi A. A decoupled impedance observer for a variable stiffness robot. *2011 IEEE International Conference on Robotics and Automation*. IEEE; 2011;5548-5553.

32. Ma H, Ren H, Zhou Q, Li H, Wang Z. Observer-based neural control of N-link flexible-joint robots. *IEEE Trans Neural Netw Learn Syst*. 2022;35(4):5295-5305.

33. Paine N, Oh S, Sentis L. Design and control considerations for high-performance series elastic actuators. *IEEE/ASME Trans Mechatron.* 2014;19(3):1080-1091.

34. Phan VD, Vo CP, Dao HV, Ahn KK. Actuator fault-tolerant control for an electro-hydraulic actuator using time delay estimation and feedback linearization. *IEEE Access.* 2021;9:107111-107123.

35. Kamalesh MS, Senthilnathan N, Bharatiraja C. Design of a Novel Boomerang Trajectory for sliding mode controller. *Int J Control Autom Syst.* 2020;18(11):2917-2928.

36. Tuan LA, Cuong HM, Trieu PV, Nho LC, Thuan VD, Anh LV. Adaptive neural network sliding mode control of shipboard container cranes considering actuator backlash. *Mech Syst Signal Process.* 2018;112:233-250.

37. Wen-Hua C, Ballance DJ, Gawthrop PJ, Reilly JO. A nonlinear disturbance observer for robotic manipulators. *IEEE Trans Ind Electron.* 2000;47(4):932-938.

38. Khalil HK. *Nonlinear Systems.* Prentice Hall; 2002.